Viscoelastic Properties of Microgel Thin Films Control Fibroblast Modes of Migration and Pro-fibrotic Responses

Daniel Chester[1,2], Rahul Kathard[1], Jeremy Nortey[1], Kimberly Nellenbach[1,2], Ashley C. Brown[*1,2]
[1]Joint Department of Biomedical Engineering, North Carolina State University and University of North Carolina at Chapel-Hill, Raleigh NC; [2]Comparative Medical Institute, North Carolina State University, Raleigh NC

[*]Corresponding Author
Ashley C. Brown, PhD
Joint Department of Biomedical Engineering
North Carolina State University and University of North Carolina at Chapel-Hill
911 Oval Drive
4204B Engineering Building III
Raleigh, NC 27606
(919) 513-8231
aecarso2@ncsu.edu

Keywords: microgels, colloidal thin film, fibroblasts, mechanotransduction, self-healing

Abstract:

Cell behavior is influenced by the biophysical properties of their microenvironments, and the linear elastic properties of substrates strongly influences adhesion, migration, and differentiation responses. Because most biological tissues exhibit non-linear elastic properties, there is a growing interest in understanding how the viscous component of materials and tissues influences cell fate. Here we describe the use of microgel thin films with controllable non-linear elastic properties for investigating the role of material loss tangent on cell adhesion, migration, and myofibroblastic differentiation, which have implications in fibrotic responses. Fibroblast modes of migration are dictated by film loss tangent; high loss tangent induced ROCK-mediated amoeboid migration while low loss tangent induced Rac-mediated mesenchymal cell migration. Low loss tangent films were also associated with higher levels of myofibroblastic differentiation. These findings have implications in fibrosis and indicate that slight changes in tissue viscoelasticity following injury could contribute to early initiation of fibrotic related responses.

Introduction:

The mechanics of a cell's biophysical microenvironment can influence cellular behavior in a number of ways. For example, substrate stiffness has been shown to modulate the attachment, proliferation, and differentiation of a number of cell types[1–3]. In order to study these phenomena, linear elastic materials, such as polyacrylamide gels, are commonly used but unfortunately do not exhibit the same time-dependent and non-linear elastic responses as biological tissues[4]. Therefore, there has been great interest in elucidating the role of non-linear material properties in controlling cellular phenotypes. Recent studies have shown that materials with differing viscoelastic properties are capable of directing cellular mechanotransduction responses irrespective of substrate stiffness[5]. Studies by Cameron et al. found that hydrogels with constant elastic moduli, but varying loss moduli, increase mesenchymal stem cell adhesion, proliferation, and differentiation rates compared to cells seeded on a purely elastic substrates with the same stiffness[6,7]. Furthermore, these responses extend to other cell types; myoblasts[8], chondrocytes[9], endothelial cells[10], and epithelial cells[11] also show increased adhesion, spread area, and proliferation on non-linear elastic substrates when compared to a purely elastic substrates of the same elastic modulus. These results also indicate that stiffness alone is not a robust enough characterization of non-linear elastic materials since cellular responses can change with small changes in viscoelasticity. Therefore, there exists the fundamental need for the development of materials with highly controllable viscoelastic properties to further elucidate the role these properties play in mechanotransduction.

Having a material platform that can accurately model nuanced viscoelastic changes in a cell's microenvironment could also be useful to elucidate the dynamics behind more complex biological processes, such as fibrosis. Fibrosis is characterized by the formation of scar tissue, which leads to overall tissue stiffening and has been shown to influence cellular responses such as migration, protein expression, and cytokine activation/signaling. Increased substrate stiffness leads to the generation of higher traction forces, increased mesenchymal cell migration rates, and increased expression of smooth muscle α-actin (α-SMA) which enhances cell contractility and promotes fibrosis[12–14]. Additionally, increased cell

contractility can lead to activation of transforming growth factor beta (TGFβ), which contributes to myofibroblastic differentiation and fibrotic responses[15–17]. Lastly, fibrosis-associated growth factors, such as connective tissue growth factor (CTGF), are increased on stiff substrates[18]. However, it remains unclear how these processes are altered at the onset of fibrosis and how diminished tissue viscoelasticity may play a roll.

Here we present the use of microgel thin films as a tunable material platform for investigating the role of viscoelastic properties in modulating cell adhesion, migration responses, and fibrosis-associated gene expression. Poly(N-isopropylacrylamide)-co-(acrylic acid) (pNIPAm-co-AAc) microgels can be fabricated into thin films through layer-by-layer (LBL) assembly with alternating deposition of positively charged linear polyelectrolytes, such as polyethylenimine (PEI). Previous studies have demonstrated that these films display non-linear properties as evidenced by the ability of certain compositions of microgel thin films to self-heal following damage[19]. The self-healing ability of the microgel films diminishes upon covalent cross-linking of microgels and linear polyelectrolyte[20], suggesting that microgel film self-healing is due to the mobility of polymer chains within the films. Additionally, the cross-linking density of microgel films influences cellular attachment[21,22]; cellular attachment was greatest on non-healing monolayers and highly cross-linked films while less cross-linked, more viscous films had less cellular attachment. These previous studies highlight the potential of using microgel thin films as a tunable platform for investigating the effect of viscoelastic properties on cell mechanotransduction responses.

Microgels are polymerized hydrogel particles that can range from nanometers to micrometers in size and have highly tunable properties. By changing the individual constituents of the microgel particles, it is possible to control particle size and mechanical properties. High degrees of tunability compounded with the film's ability to interact and influence cellular behavior, makes these films an ideal material platform to study how substrate viscoelasticity influence mechanotransduction responses. We hypothesize that microgel film viscoelasticity can be controlled by altering the degree of internal cross-linking within the microgel particles, without significantly changing their elastic modulus, and can therefore be used to

study the mechanisms by which cells sense and respond to the non-linear properties of their biophysical environment. Here we investigate this hypothesis by characterizing the effect of microgel cross-linking on film viscoelasticity. We then demonstrate that film self-healing dynamics and corresponding viscoelastic properties correlate with fibroblast spreading, modes of migration, and fibrosis-associated protein expression dynamics.

Results:

Characterization of microgel thin films with controllable viscoelastic properties

To modulate colloidal film viscoelastic properties, we synthesized negatively charged microgels with varying degrees of N,N'-Methylenebisacrylamide (BIS) cross-linking and then fabricated the microgels into 4-layer thin films. Microgel particles were synthesized with either low (1% BIS), intermediate (2-4% BIS), or high (7% BIS) internal cross-linking densities. 4 layer films were chosen because this number of layers has previously been shown to display self-healing responses, while microgel monolayers do not [23] and cellular responses measured on microgel monolayers did not statistically differ from glass (**Sup. Fig. 1**). Nanoparticle tracking analysis (NTA) of the microgels showed that the mean hydrodynamic diameter of the particles was 567±34 nm (**Fig. 1; Sup. Fig. 2**). DLS measurements of microgel hydrodynamic radius over the temperature range of 25-45 °C show that below 35° C all microgel particles had sizes between 500-600 nm and above 35 °C all microgel particles had sizes between 300-400 nm (**Sup. Fig. 3**). This indicates that the volume phase transition temperature of each microgel composition is similar even though the percentage of pNIPAm differs slightly between each formulation. Atomic force microscopy (AFM) height traces showed increasing particle heights as cross-linking percentage increased with the lower cross-linked particles having four times shorter particle heights than higher cross-linked particles, despite having similar diameters. The difference in microgel particle heights is an indication of their deformability, where lower cross-linked particles appear to spread more on a glass surface while higher cross-linked particles act more as hard spheres and do not spread extensively[24–26].

AFM nanoindentation demonstrated that film elastic modulus was approximately 107±18 kPa for all films (**Sup. Fig. 4**). A slight increase in modulus was observed with increasing particle cross-linking, but the differences were not statistically significant. Surface roughness calculations of the microgel thin films showed that the arithmetic mean deviation (Ra) of the surface features were less than 50 nm on all films and no statistical differences were observed between film types (**Fig. 1; Sup. Fig. 5**). The swelling capacity of the microgel films was also measured, and all films had dry film thicknesses of ~500 nm and hydrated film thicknesses of ~1500 nm with no statistical differences observed between films (**Sup. Fig. 6**). To determine how properties of the films change during film build-up, we analyzed surface coverage and mechanics following the addition of each layer for 2% BIS films (**Sup Fig. 7; Sup. Fig 8**). It was found that as each layer was added, surface coverage improved until no glass or individual microgel particles could be seen and stiffness decreased with increasing layer number.

A summary of the particle hydrodynamic diameter, dry heights, surface roughness, and compressive moduli of the microgel films are shown in **Fig. 1**. We next characterized the self-healing and viscoelastic properties of the films. A self-healing assay showed that as the intraparticle cross-linking density increased, film self-healing responses were diminished (**Sup. Fig. 9**). Lower cross-linked films exhibited greater healing responses than higher cross-linked films, indicating a higher degree of polymer mobility and more viscous materials. We next measured film loss tangent, which is a measure of the ratio between a materials loss modulus to its storage modulus, and for materials with similar storage modulii, is often used as an indication of material viscosity[5]. There is an inverse relationship between film loss tangent and intra-microgel cross-linking (**Fig. 1**); higher intra-microgel cross-linking densities correlates with lower film loss tangents and lower film viscoelasticity. The loss tangent values of the microgel films significantly decreased with increased particle cross-linking ($p<0.05$) and ranged from 1.8±0.1 for 1% BIS films to 0.8±0.2 on 7% BIS films (**Sup. Fig. 10**). These values were seen to be consistent for 3 different areas on 3 different films from different batches indicating that the viscoelastic properties of the films are homogenous across the film surface and between fabrication batches. We ran a correlation

analysis to further explore the relationship between microgel %BIS and the resulting loss tangent/ Young's modulus of the films (**Sup. Fig. 11**); a strong, statistically significant, linear correlation exists between loss tangent and %BIS, while a weak, not statistically significant, linear correlation exists between Young's modulus and %BIS and between Young's modulus and loss tangent.

Quantification of fibroblast spreading and migration rates on microgel thin films

To analyze the influence of film loss tangent on cell migration, human dermal neonatal fibroblasts (HDFns) were seeded on collagen coated microgel films and imaged over a 24-hr period **(Sup. Videos 1-5)**. Image stacks were processed in ImageJ and analyzed in the cell tracking software Aivia[27] to quantify cell velocity, path length, and straight-line length (**Fig. 2)**. Path length is defined as the length of the path taken between each consecutive time interval from the beginning to the end of the tracking period and straight-line length is defined as the shortest distance between the first and last frame of the track. As film loss tangent decreased, cellular velocity, path length, and straight-line length increased. The differences in migration on the low loss tangent and high loss tangent films correlated with two different modes of cell migration (amoeboid or mesenchymal). In amoeboid migration, cells change shape rapidly by sending out many protrusions and then rapidly migrate large distances, which correlates with the low path lengths and high straight-line lengths observed. In mesenchymal migration, cells have distinct leading and trailing edges and migrate in a more stepwise fashion correlating with higher path lengths and straight-line lengths. **Figure 2A** further visualizes the different modes of migration by showing representative migration patterns of the cells seeded on microgel films with varying cross-linking densities, which correspond with the description of amoeboid and mesenchymal cell migration.

Increased material elastic modulus has previous been shown to lead to increased cell spreading[28], increased myofibroblastic differentiation[29], and increased expression of fibrosis related genes such as α-SMA and CTGF[30]. We were therefore interested in characterizing how these responses correlate with loss tangent on our films with stiff elastic moduli. HDFns were cultured on microgel thin films with varying loss tangents for 24 hrs, then fixed and stained for α-SMA and CTGF (**Fig. 3**). Cell

area and circularity was measured in ImageJ, and it was found that cell area on high loss tangent films increased significantly compared to low loss tangent films. Cell circularity was also highest on the intermediately cross-linked, low loss tangent films. Quantification of α-SMA expression showed no significant differences in overall expression between films, however the percentage of stress fiber positive cells, indicative of myofibroblastic differentiation, was seen to increase as film loss tangent decreased. It was found that the highest amounts of CTGF expression occurred on the intermediate cross-linked films with lower loss tangent values, and were significantly different than the amount of CTGF expression measured in the other conditions. Staining for paxillin and FAK also indicated that on lower cross-linked films, weak focal adhesions seem to be localized around edges of the cell as seen by the diffuse staining around the edges of the cell, while on the higher cross-linked films stronger focal adhesions can be seen to be localized around the center of the cell (**Sup. Fig. 12**). These results indicate that fibroblasts tend to have a more myofibroblastic phenotype when seeded on films with lower loss tangent values as seen by increased cell areas, stress fiber positive cells, and CTGF expression.

Since cell spreading and migration are contractility mediated responses, we next quantified cell contractility following incubation for 12 hrs on microgel thin films using both AFM single cell stiffness measurements and traction force microscopy (TFM) to measure the amount of tension forces generated by cells (**Fig. 3**). As film loss tangent decreased, mean single cell stiffness increased significantly from 0.3±0.1 kPa on the 1% BIS films to 1.4±0.2 kPa on the 7% BIS films ($p<0.05$; **Sup. Fig. 13**). TFM results demonstrated that cells seeded on control surfaces, i.e. PA gels without film coatings, generated significantly more traction than cells cultured on film-coated surfaces (**Sup. Fig. 14**). Results, from TFM did not result in significant differences between films, however cells were able to generate traction forces ranging from 100-250 Pa on the film-coated surfaces, while traction forces averaging 750 Pa were measured on control surfaces. It is possible that differences in traction forces could be greater at earlier timepoints. Due to the viscoelastic nature of the films, after 12 hrs it is possible that creep could have occurred causing the bead position to relax and move closer to its original location and result in lower

traction forces. Furthermore, since the fluorescent beads are embedded in the PA gel and not in the microgel film, it is possible that the system is not sensitive enough to pick up smaller traction forces generated by cells seeded on the microgel layers.

Cell contractility inhibitors normalize cell spreading and migration responses on microgel thin films

To determine the influence of GTPase signaling on the observed responses, cell migration, spreading, and protein expression were analyzed on microgel films in the presence of Rac, ROCK, and CDC42 inhibitors (**Fig. 4**; **Fig. 5; Sup. Videos 6-20**). The addition of each inhibitor was found to normalize cellular migration velocity across all conditions. Addition of the ROCK and CDC42 inhibitor significantly increased total cell migration, as both the straight-line length and path length of the cells were increased in the presence of ROCK and CDC42 inhibitors, however the magnitude of these responses in the presence of the CDC42 inhibitor were not as stark as those observed in the presence of the ROCK inhibitor. Finally, the addition of the Rac inhibitor greatly reduced all migration responses as both straight-line length and path length were significantly reduced.

Inhibition of Rac was also found to significantly decrease cell spread area while increasing cell circularity after 24 hrs, while inhibition of ROCK and CDC42 appeared to normalize both cell spreading and circularity across all conditions. Rac inhibition also significantly decreased the amount of stress fiber positive cells, while both CDC42 and ROCK inhibition normalized the amount of stress fiber positive cells on all films. Finally, across all conditions, CTGF expression was normalized with the addition of all of the inhibitors. Overall, with the addition of the cell contractility inhibitors, the responses due to differences in film loss tangent were no longer apparent. Addition of all of the inhibitors normalized migration velocity, while addition of the ROCK inhibitor was seen to increase total cell migration, and the addition of a Rac inhibitor significantly diminished spreading responses.

Outlook and implications in fibrotic responses:

In these studies, we demonstrate that microgel thin films are a tunable platform with controllable loss tangent properties and film loss tangent drives fibroblast modes of migration and contributes to pro-

fibrotic responses. To ensure that the cellular responses measured were due primarily to the differences film loss tangent values, a robust characterization of both the microgel particles and films was first performed. Microgel particles were similar in size (~600 nm in diameter), films had similar compressive modulii (~100 kPA), and the average surface feature of each film was less than 50 nm. Previous work has shown that fibroblast adhesion and spreading responses plateau on substrate stiffnesses greater than 50 kPa[3]; with a mean stiffness of 107±13 kPa, our films are above this threshold, therefore, any observed differences in cellular responses should be primarily due to the differences in loss tangent.

We first characterized film viscoelasticity using a film self-healing assay and results showed that as intraparticle cross-linking density increases, the ability for the films to heal decreases. These results corroborate previous work demonstrating that inter-microgel cross-linking decreases microgel thin film's self-healing ability[20] by restricting the ability of polymer chains to move and rearrange. Intraparticle cross-linking appears to result in a similar effect, which is likely due to the decreased mobility of polymer chains within individual microgel particles with increasing intraparticle cross-linking. Loss tangent imaging demonstrated that increasing intraparticle cross-linking density led to lower loss tangent values. A correlation analysis between loss tangent and microgel %BIS showed a strong correlation between the two parameters (**Sup. Fig. 11**). These results showed that microgel particles are highly tunable, as both the size and stiffness can be controlled during synthesis and used to create films with different viscoelastic properties.

Loss tangent imaging showed that our films had loss tangent values over the range of 1.8 to 0.8. Other studies performing AFM based imaging to find the loss tangent values of biological cells or tissues can help put these values into a relevant biological context. Loss tangent values for sheep aorta were found to be 1.0 in young sheep and decreased to 0.86 in aged sheep[31]. Loss tangent values for the benign cell types NIH 3T3, MDCK-II, NMuMG, and MCF-10A all fell within the range of 1.0-1.5, while loss tangent values for malignant cell types SW-13, A549, MCF-7, MDA-MB-231, and CaKi-1, all fell within the

range of 1.5-3.0[32]. Also, loss tangent values of human lung epithelial cells have been measured at ~0.5[33].

Other methods, including dynamic material analysis and contact resonance, have been used to measure the loss tangent values of biological tissues, however these methods have been shown to provide values that are much lower than those measured by AFM[34]. This has been attributed to the differences in the frequency to which the material responds, which for AFM can be 10-100 kHz, compared to the frequency of 1-100 Hz used commonly by other methods. As such, it is not accurate to directly compare values obtained by other methods to the measured values of our films, however the trends observed through other methods remain relevant. For example, studies by Yin et al. found the loss tangent value of a mouse liver following injury and before fibrosis was ~0.1 and then decreased to ~0.03 at the onset of fibrosis, which was lower than the measured healthy tissue loss tangent of ~0.06[35], indicating that decreased loss tangent could contribute to fibrotic responses *in vivo*. Indeed, our studies investigating the effect loss tangent on cell migration and fibrosis related responses supports this hypothesis.

Analysis of cell migration on microgel films showed that velocity, path length, and straight-line length increased as loss tangent decreased. This quantification, in conjunction with detailed observation of the time-lapse videos, indicates that two different modes of migration are occurring. These two modes of individual cell migration have been well characterized and are described as amoeboid and mesenchymal cell migration. Amoeboid migration is characterized by rounded or ellipsoid cells that do not have mature focal adhesions or stress fibers and, during locomotion, change shape by rapidly protruding and retracting filopodia[36,37]. Amoeboid migration is also associated with cancer cell infiltration and metastasis[38]. This is particularly interesting as the loss tangents of malignant cell lines are similar in value to the lower cross-linked microgel films in which amoeboid migration was also observed, indicating a potential link between substrate loss tangent and cancer cell infiltration and metastasis. On the other hand, mesenchymal migration is characterized by elongated, polarized cells that contain a leading edge with protrusions leading to the new site of migration and a trailing edge that retracts upon initiation of migration[39].

Interestingly, mesenchymal migration is promoted on stiffer substrates and has been associated with fibrotic responses[40].

In our studies, we observed that on 1% BIS films, corresponding to the highest loss tangent value, filopodal amoeboid cell migration occurs, while on 7% films, corresponding to the lowest loss tangent value, mesenchymal migration occurs. On 2% and 4% BIS films, corresponding to the intermediate loss tangent values, a transition between amoeboid and mesenchymal migration occurs. On 1% films, an inverse relationship between path length and straight-line length is observed, which supports the conclusion that amoeboid migration is occurring. Since path length is the measurement of the total distance traveled and straight-line length is the measure of the shortest distance between the start and end of the track, having a cell that is not moving but instead sending out many protrusions will lead to a lower average path length per cell, and will concurrently lead to a larger straight-line length due to the large distances traveled during one of the quick migratory movements characteristic of amoeboid migration[39]. More elongated, ellipsoid cells with decreased cell areas were observed on the lower cross-linked films due to the short lived and loose interactions with the substrate, preventing the cells from generating sufficient internal tensional forces needed for spreading. These observations were also confirmed by characterizing focal adhesion formation after 24 hours (**Sup. Fig. 12**), where diffuse staining of paxillin and FAK around the edge of the high loss tangent films indicates weak focal adhesion formation. Additionally, lower amounts of stress fiber positive cells were observed on lower cross-linked films, which is also a key characteristic of amoeboid migration. Furthermore, single cell force mapping showed lower cell stiffness on the lower cross-linked films, which is expected in cells that are loosely attached to the surface. Collectively, our data indicates that materials with higher loss tangent drive amoeboid migration.

On the 7% BIS cross-linked films, corresponding to the lowest loss tangents, mesenchymal cell migration was observed. This conclusion is supported by greater rates of migration, increased spread area, and increased cell stiffness observed on these films, compared to the 1% BIS cross-linked films. Due to the low viscosity of these films, cells are able to actively polarize into a trailing and leading edge, which

allows for more step-wise migration leading to longer pathlengths. Cells are also able to generate larger internal tensional forces, which leads to greater spread areas, stress fiber formation, and cell stiffness values. The ability for cells to generate larger tensional forces was also confirmed by the staining of paxillin and FAK on the low loss tangent films indicating strong focal adhesion formation (**Sup. Fig. 12**). On the 2% and 4% BIS films, corresponding to the intermediate loss tangent values, a transition from amoeboid to mesenchymal migration is observed. This conclusion is supported by the range of morphology and migratory responses measured on these films.

Taken together, these results show that substrate loss tangent can modulate cell migration by determining the mode by which cells migrate where loss tangent values lower than 1.4-1.5 promote mesenchymal migration, loss tangent values greater than 1.4-1.5 promote amoeboid migration, and loss tangent values of 1.4-1.5 promote the transition between the two modes of migration. These results are also supported by the aforementioned loss tangent values of epithelial, benign, and malignant cells which were found to be 0.5, 1.0-1.5, and 1.5-3.0 respectively. For single epithelial cells, mesenchymal migration is the normal mode of migration[41] and for cancer cell metastasis amoeboid migration is the most commonly found mode of migration[42,43] which further demonstrates that a loss tangent values of 1.4-1.5 lead to a transition between the two modes of migration. On the material level, loss tangent values greater than 1.5 cause the films to flow away from the cell as it exerts a force on the film. Due to the movement of the film in the direction away from the cell, the cell is unable to generate internal tensional forces sufficient enough to allow for large spread areas. The inability to spread inhibits the cell from polarizing to form a leading and training edge resulting in amoeboid migration. However, loss tangent values lower than 1.4 provide enough resistance within the film to prevent the movement of the film away from the cell. This allows for the cell to obtain the internal tensional forces required for larger spread areas. With sufficient enough internal tensional forces, the cell can then polarize to form a leading and trailing edge and undergo mesenchymal migration. Focal adhesion staining also shows a more diffuse

staining around the periphery of the cell on the lower cross-linked films and more robust staining by the nucleus of the cell on the higher cross-linked films (**Sup. Fig. 12**).

Since cell contractility plays a major role in both cell migration and spreading, cellular responses were characterized in the presence of the GTPases inhibitors Rac, ROCK, and CDC42. In general, the addition of the contractility inhibitors had a normalizing effect and eliminated any differences observed due to the changes in the loss tangent values between the microgel films. However, the effects from inhibiting Rac indicate that it is a crucial pathway contributing to the mesenchymal migration observed on lower loss tangent films (**Sup. Fig. 15**). Previous reports by *Cameron et al*. also identified the importance of Rac1-mediated signaling in responses of mesenchymal stem cells on hydrogels with variable rates of creep; in those studies, increased Rac1 signaling was observed on high creep hydrogels where spread area, migration, and differentiation was also the highest. High Rac signaling is also known to increase leading edge extension, elongated morphology, integrin engagement, and mesenchymal migration[44–46]. However, ROCK signaling in the absence of Rac has been shown to increase the rounded cell shapes associated with amoeboid migration[44], which also matches the increase in rounded cell shapes and cell circularity we observed on microgel films upon the addition of a Rac inhibitor. These results further indicate that Rac mediated signaling is an important factor for directing mesenchymal cell migration on low loss tangent films since amoeboid cell migration is observed in the absence of Rac.

The effects from inhibiting ROCK indicate that it is a crucial pathway contributing to both the mode and rate of migration on microgel thin films with varying loss tangents. Studies by *Totsukawa et al*. showed that fibroblast cells cultured on glass coverslips and treated with a ROCK inhibitor migrated further and in a straighter direction than untreated fibroblasts[47]. Similarly, our results obtained for cell migration on microgel films in the presence of ROCK inhibition showed greater path lengths and straight-line lengths when compared to cells on films with the identical loss tangent values, but different inhibitory conditions. Previous reports have also shown that high Rac activity in the absence of ROCK further promotes elongation and mesenchymal migration; likewise, we observed an increase in area and migration

rates of cells that underwent ROCK inhibition on films that otherwise supported amoeboid migration (**Fig. 4; Sup. Fig. 16**)[45]. It was also found that ROCK inhibition significantly increased migration and spread area on high loss tangent films where amoeboid migration was the dominant mode of migration when compared to low loss tangent films where mesenchymal migration was already the dominant mode of migration (**Sup. Fig. 17**). These results further indicate that ROCK mediated pathways are critical for directing amoeboid cell migration on films with low loss tangents since mesenchymal cell migration is observed in the absence of ROCK.

CDC42, along with Rac, is involved in controlling the filipodia dynamics at the leading edge during cell migration[48]. If Rac and CDC42 worked in conjunction with one another during mesenchymal migration on the microgel films, then it would be expected that inhibition of CDC42 would yield similar results to the inhibition of Rac. However, the converse was observed and inhibition of CDC42 yielded similar results to inhibiting ROCK on microgel films (**Sup. Fig. 18**). Inhibition of CDC42 led to cells with increased spread areas, stress fibers, and migration distances, but the magnitude of these observations was not as great as with ROCK inhibition. It was also observed that inhibiting CDC42, similar to when ROCK was inhibited, resulted in a significant increase in migration and spread area on high loss tangent films where amoeboid migration was dominant when compared to low loss tangent films where mesenchymal migration was dominant (**Sup. Fig. 17**), although the magnitude of the increase was not as great as when ROCK was inhibited. These results suggest that CDC42 plays a more important role in controlling filipodia dynamics at the leading edge during amoeboid migration and a smaller role during mesenchymal migration on microgel films. However, it appears that ROCK is the more dominant pathway controlling amoeboid migration. The previously reported results, combined with our own, further identify both Rac and ROCK as the dominant pathways in measuring and responding to viscoelastic substrates.

The observations that small changes in substrate viscoelasticity have such a large effect on cell migration and morphology have broader implications for more complicated processes such as the propagation of fibrosis. Previous studies have shown that substrate stiffness plays a significant role in the

propagation of fibrosis with higher rates of fibrosis found on stiffer substrates[15,49,50]. Furthermore, ROCK has been identified as a key driver in fibrotic related responses. Upregulation of ROCK has been shown to increase fibroblast contractility[29,51], increase fibrotic responses[16], and increase the length and severity of fibrotic responses[15]. Our results suggest that such responses might be more nuanced than just a straightforward increase in ROCK expression or substrate stiffness. For example, slight changes in substrate viscoelasticity could cause cells to transition from amoeboid to mesenchymal cell migration modes leading to an increase in actin stress fiber formation, cell spread area, and other myofibroblastic phenotypes, thereby resulting in an increase in ECM deposition and accelerating fibrotic responses. It is possible that slight changes in tissue viscoelasticity following injury could lead to initiation of fibrotic related responses, however more research on this topic is needed.

Additionally, the role that substrate stiffness has on the propagation of fibrotic related responses has been well characterized, however, these studies have predominately utilized linear elastic materials. Our studies highlight that it is not sufficient to only consider elastic modulus and that loss tangent is also an important descriptor for such responses. Further studies are needed to fully understand the combinatory effects that substrate stiffness and loss tangent have on cellular responses and the initiation of fibrosis. To begin to probe these complex interactions, we built microgel thin films on top of PA gels with Young's moduli of 8.8 kPa. Initial results (**Sup Fig. 19**) do show differences in the cell area of fibroblasts seeded on such substrates when compared to fibroblasts cultured on microgel films built on glass, further exemplifying the need to investigate the complex relationship between substrate stiffness and film loss tangent on cellular responses in greater detail.

Overall, we have shown that microgel thin films can be constructed to have differential viscoelastic properties and can be used as a platform to study how these properties influence cellular behavior. Specifically, as film loss tangent decreased, cell area, circularity, stress fiber formation, and CTGF expression increased, while migration transitioned from amoeboid to mesenchymal (**Fig. 6**). In the presence of cell contractility inhibitors, it was found that inhibiting Rac had the greatest effect on the high

loss tangent films, while inhibiting ROCK and CDC42 had the greatest effect on the low loss tangent films further indicating that Rac is an important pathway in mesenchymal migration and ROCK and CDC42 are important pathways in amoeboid migration. While these results begin to provide some insight into the effects that material viscosity has in modulating cellular behavior, much remains to be fully elucidated. Overall, we demonstrate that microgel thin films provide a highly tunable, easily synthesized material platform for further elucidating such responses and have the potential to be used as a platform to build substrates with specific properties to elicit desired cellular responses.

Materials and Methods:

All reagents were purchased from Sigma-Aldrich unless otherwise noted.

Microgel Synthesis and Purification

Microgel particles were synthesized in a precipitation-polymerization reaction. Poly(N-isopropylacrylamide) (poly-NIPam), N,N'-methylenebis(acrylamide) (BIS), Acrylic Acid (AAc), and sodium dodecyl sulfate (SDS) were added to 95mL of de-ionized water and added to a three-necked reaction vessel, where it equilibrated at 70^{o}C for one hour. Ammonium persulfate (APS) was added to initiate the reaction. The reaction was allowed to proceed for 6 hours at 70^{o}C and a stir speed of 450 RPM and cooled overnight while continuing to stir. Once cooled, the solution was filtered over glass wool to remove any microgel aggregates and then transferred to 1000 kDa dialysis tubing (Spectrum Laboratories). Water for dialysis was changed every 12-16 hours over the course of 48 hours and microgels were then freeze dried. Microgel composition was varied by keeping the amount of Aac constant at 5%, varying the amount of BIS to be either 1, 2, 4, or 7%, and then calculating the remaining percentage of Poly-NIPAM. SDS was added in order to control the size of the microgel particles.

Microgel Size characterization

Microgel particle hydrodynamic radius was measured using nanoparticle tracking analysis using a NanoSight (Malvern). Microgel particle hydrodynamic radius as a function of temperature was measured with dynamic light scattering (Malvern Zetasizer Nano S) over the range of 25-45 °C. Microgel heights

were measured using a MFP-3D atomic force microscope (AFM; Asylum) in AC mode with ARROW-NCR cantilevers (Nano and More USA) with a spring constant of 42 N/m.

4 Layer Thin Film Construction

Microgel thin films were fabricated through active centrifugal deposition in a layer-by-layer fashion on glass coverslips by alternating layers of microgel solution with poly(ethyleneimine) (PEI)[52,53]. The glass coverslips were first functionalized in a solution of 1% (3-Aminopropyl)trimethoxysilane (APTMS) in absolute ethanol for 2 hours and washed once with DI water. Then, a 0.1 mg/mL solution of the microgel particles was added to the functionalized coverslip and centrifuged a 3000xg for 10 minutes. The solution was then removed and the coverslips were washed 3 times in DI water for 5 minutes. A solution of 0.05 monomolar PEI was then added and shaken at room temperature for 30 minutes. The PEI solution was removed and the coverslips were then washed 3 times in DI water for 5 minutes. This process was then repeated 3 more time for a total of 4 microgel layers with the last layer of the film being a layer of the microgel particles.

4 Layer Thin Film Characterization

The surface coverage, surface roughness, and Young's Moduli of the constructed microgel films were characterized using a MFP-3D AFM (Asylum). To measure the surface coverage of the films after each layer, ARROW-NCR cantilevers (Nano and More USA) with a spring constant of 42 N/m were used in AC mode and a 20x20 μm area was imaged after each film was built. To calculate surface roughness, ARROW-NCR cantilevers (Nano and More USA) with a spring constant of 42 N/m were used in AC mode. Then, 3 90x90 μm areas were measured in 3 different locations on 3 different films for a total of 9 images per film. The arithmetic mean deviation (Ra) of each film was then calculated using the AFM software. To measure the swelling capacity of the 4-layer microgel films, a razor blade was used to scratch the films and film thickness was measured while the films were dry and hydrated using AFM [54,55]. Two 90x90 micron scratch areas were imaged on 3 different films for a total of 6 film thickness values per film. To measure the Young's Modulus of film layers and completed films measurements were made

with PNP-TR cantilevers with a pyramidal tip geometry and a cantilever constant of 0.08 N/m (Nano and More USA) were used in contact force mode. An area of 10 x 10 μm was used for the force maps with a total of 256 force curves being measured in the selected area. A total of three different spots were measured on each film tested and three different films from three different microgel film batches were used. The resulting indentation curves were then fit with the Hertz model using analysis software from Asylum. Loss tangent imaging was performed using a Cypher ES AFM (Asylum) and BL-AC40TS-C2 cantilevers (Olympus) with a cantilever constant of 0.09 N/m. An area of 5x5 μm was used and three different locations were measured on each film. A total of 3 different films from 3 different batches were used to give a total of 9 loss tangent values for each film.

4-Layer Thin Film Self-Healing Analysis

Previous studies have shown that uncross-linked microgel thin films constructed from 4% BIS microgels undergo rapid self-healing, while identical films cross-linked to the PEI chains through EDC/NHS cross-linking do not[21]. We therefore, were interested in characterizing the role of interparticle BIS cross-linking, within non-cross-linked thin films, on modulating film self-healing ability. Microgel self-healing experiments were therefore performed on 4-layer thin films created on polydimethylsiloxane (PDMS)[20,24,54]. PDMS was made using a mixture of nine parts elastomer to one-part curing agent and placed in a vacuum desiccator for 20 minutes to remove any air bubbles. The PDMS was then allowed to cure for 24 hours at room temperature and then cut into 9x18 mm strips. In order to remove any uncured PDMS and prepare the PDMS for surface functionalization, the PDMS strips were submerged in hexanes for 2 hours at room temperature and then drained and heated at 50^{o}C for 2 hours to evaporate any remaining hexanes followed by incubation in 1.2M HCl for 16 hours at room temperature. Upon removal, the strips were washed three times with DI water, twice with absolute ethanol, and then shaken at room temperature in absolute ethanol for 30 minutes. The PDMS strips were then functionalized with APTMS and 4-layer thin films constructed as previously described. To perform the self-healing experiments, the 4-layer thin films on PDMS were imaged dry using a MFP-3D AFM (Asylum) in AC mode with ARROW-

NCR cantilevers, with a pyramidal tip geometry and a cantilever constant of 42 N/m, (Nano and More USA) before damage, after damage, and after healing. Damage was induced by taking a micropipette tip and scratching the surface of the film until there was a visible white line. Microgel film healing was then controlled through steam exposure and films were exposed to steam for <1 second, 1 second, or 5 seconds.

Dynamic Cell Migration and Spreading Experiments

4-layer microgel films were sterilized in a solution of 20% ethanol for 30 minutes before being washed in sterile phosphate buffered saline (PBS) and incubated in sterile PBS at room temperature for 24 hours. The films were then coated in type I rat tail collagen (Fisher Scientific) at a concentration of 10 $\mu g/cm^2$ in sterile PBS overnight at 4^oC. An empty 12-well plate was then coated in 1% bovine serum albumin (BSA; Fisher Scientific) overnight at 4^oC to block non-specific cellular attachment to the well plate. The collagen coated films were adhered to the BSA coated well plate using a glass epoxy (VWR) in order to prevent the movement of the films throughout the experiment. The glass epoxy was tested prior to use to ensure that there were no cytotoxic effects by first seeding cells on glass coverslips coated with collagen with cured epoxy exposed to the cell culture media. A live/ dead assay was performed on glass coverslips with and without the epoxy present and there were no statistical changes in cell viability measured (**Sup. Fig. 20**). Neonatal human dermal fibroblasts (HDFns; Gibco) were then seeded onto the films at a density of 12-15k cells/ cm^2 and imaged every 500 seconds at a temperature of 37^oC and compiled into image stacks using ImageJ and analyzed in the software AIVA (DRVision). In the experiments where an inhibitor was use, the inhibitor was added 2 hours after seeding the cells on the films. Concentrations used for each inhibitor is as follows: ROCK inhibitor Y-27632 (Fisher Scientific) added at a concentration of 10 μM[47,56], Rac inhibitor CAS 1177865 (Fisher Scientific) added at a concentration of 100 μM[57], and CDC-42 inhibitor ML141 (EMD Millipore) added at 10 μM[58]. For each experiment, cell behavior was analyzed on thin films constructed from 1, 2, 4, and 7% BIS microgels; a collagen-coated glass coverslip was used as a control.

Analysis of Cell Spreading

4-layer films or monolayers were sterilized and collagen coated in the same manner as the films used in the dynamic experiments. HDFns were then seeded at a density of 15-20k cells/cm^2 and incubated for 24 hours at a temperature of 37^oC and 5% CO_2. In the experiments where an inhibitor was used, the inhibitor was added 2 hours after seeding the cells on the films at the same concentrations used in the dynamic experiments. At the end of the 24 hours, the cells were fixed and immunohistochemistry staining was performed. HDFn cells were fixed in a solution of 95% methanol (Alfa Aeser) and 5% glacial acetic acid (EMD Millipore), that was cooled to -20^oC, and placed in a -20^oC freezer for 10 minutes. The fixed cells were then washed 3 times with ice cold PBS and then permeabilized in PBS with 0.1% Tween-20 (PBST; Fisher Scientific) for 30 minutes. The cells were then blocked for 30 minutes in a solution of 5% non-fat milk (Fisher Scientific) dissolved in PBST while shaking at room temperature. Next, the cells were incubated with the primary antibodies α-smooth muscle actin (α-SMA) clone 1A4 (Fisher Scientific) and connective tissue growth factor (CTGF) clone ab6992 (Abcam) in a solution of 5% non-fat milk dissolved in PBST at a concentration of 25 μg/mL for 2 hours shaking at room temperature and then washed 3 times with PBS. Alexa-fluor 488 and Alexa-fluor 594 secondary antibodies (ThermoFisher) along with NucBlue live cell stain (ThermoFisher) were then added in a concentration of two drops per mL to a solution of 5% non-fat dry milk and incubated shaking at room temperature for 1 hour. The coverslips where then mounted on glass slides using Fluoromount G mounting media (Electron Microscopy Science) and imaged on an EVOS FL Auto (ThermoFisher). Images were then analyzed in ImageJ where area, circularity, corrected total cell fluorescence, and the percent of α-SMA positive cells were measured. To measure CTGF expression, the calculation of the corrected total cell fluorescence for each cell was found by taking the integrated density of the signal from the cell and subtraction area of the cell multiplied by the fluorescence of the background[59]. This raw value was then normalized to the average CTGF expression of the control for each experiment. In order to find the percent of α-SMA positive cells, the total cells were counted in an image and the percent of cells with α-SMA positive stress fibers was calculated.

Single Cell Force Mapping

4-lyaer microgel films were created on top of glass bottom petri dishes (World Precision Instruments) in the same manner as previously stated. The films were sterilized and collagen coated in the same manner as previously mentioned. HDFns were seeded at a density of 15-20k cells/cm^2 and allowed to attach for 12 hours at 37^{o}C and 5% CO_2. After 12 hours, the media was removed and the cells were placed in sterile PBS for AFM force mapping. Cells stiffness was measured using a MFP-3D AFM (Asylum) and CP-qp-CONT-ps cantilevers (NanoAndMore) that have a spherical tip geometry with a two-micron diameter and a cantilever constant of 0.1 N/m. Force maps were performed twice in two different spots over the cytoplasm in order to measure the stiffness of each cell and a total of 5-10 cells were measured per condition. Each force map was over a 5 μm by 5 μm area with a total of 36 force curves being measured in that area. The resulting force curves were fit with the Hertz model and analyzed in software from Asylum.

Traction Force Microscopy

Traction force microscopy was performed using a modification of standard protocols[60–64]. A solution of 0.1M sodium hydroxide (NaOH) was left to evaporate in a glass bottom 12 well cell culture plate (MatTek) before the plate was functionalized with pure APTMS for 6 minutes at room temperature while shaking. The well plates were then washed 3 times with de-ionized water (dIH2O) for 5 minutes, before being allowed to dry completely. Once dry, a 0.05% solution of glutaraldehyde in PBS was left in each well for 30 minutes followed by three more washes with dIH2O and being left to dry completely. Polyacrylamide (PA) hydrogels with polydisperse fluorescent beads were then constructed on the functionalized glass bottom plates. Solutions of 40% acrylamide and 2% BIS were mixed in dIH2O with red fluorescent beads added. The solution was initialized with 10mg/ml APS and 97% tetramethylethylenediamine (TEMED) and pipetted into the functionalized glass bottom wells before being covered with dichlorodimethylsilane (DCDMS) coated coverslips and allowed to solidify. Coverslips were functionalized through addition of 99.5% purified DCDMS under a hood and allowed to air dry for a minimum of 12 hours. Upon hydrogel solidification, the wells were filled with 4-(2-

hydroxyethyl)-1-piperazineethanesulfonic acid (HEPES) buffer and left for a minimum of 4 hours. The PA hydrogels had Young's moduli of 8.8 kPa. The coverslips were removed, and the PA hydrogels functionalized with sulfosuccinimidyl 6-(4'-azido-2'-nitrophenylamino)-hexanoate (sulfo-SANPAH) by activating a solution of 0.01mg/ml sulfo-SANPAH and 0.0083% dimethyl sulfoxide (DMSO) in HEPES buffer with UV light (254 nm) before incubating the well with 0.05 monomolar PEI overnight at room temperature. Following PA gel functionalization, 4-layer colloidal thin films were made in the layer-by-layer process described above. The thin films were then incubated with 100 μg/ml collagen in PBS for 12 hours before HDFns were seeded and left to attach for 12 hours. Following cellular attachment as well as following cell lysing with 7mM EDTA in 3% SDS solution, traction force microscopy measurements were taken and analyzed through MATLAB and ImageJ[63].

Statistical Analysis

All statistical analysis was performed in the Prism software (Graphpad). Data was statistically analyzed using either a one-way or two-way ANOVA with subgroup comparisons done using the Tukey post-hoc test at a 95% confidence interval. All results are reported as the mean ± the standard deviation. All experiments performed had a minimum of 3 replicates.

Author Contributions:

D.C. wrote and edited the manuscript, synthesized microgels, created films, designed and performed experiments, and analyzed data. R.K. synthesized microgels, created films, created the image processing code for analysis of cell migration videos, performed TFM experiments, and contributed to data analysis. J.N. synthesized microgels, created films, performed immunohistochemistry, and contributed to data analysis. K.N. performed all confocal imaging. A.C.B wrote and edited the manuscript, designed experiments, and analyzed data.

Acknowledgments:

Funding for this project was provided by NSF BMMB 1825398, the Faculty Research and Development Program at NCSU (to ACB) and the Abrams Scholars Program (to RK and JN). Authors acknowledge Dr.

Ismaeel Muhamed for his assistance with TFM and Asylum Research specialists Keith Jones, Tim Walsh, and Ryan Fuierer for their expertise in AFM imaging techniques.

Data Availability:

The raw/processed data required to reproduce these findings cannot be shared at this time as the data also forms part of an ongoing study.

References:

[1] D.E. Discher, P. Janmey, Y. Wang, Tissue Cells Feel and Respond to the Stiffness of Their Substrate, Science. 310 (2005) 1139–1143. doi:10.1126/science.1116995.
[2] A.J. Engler, S. Sen, H.L. Sweeney, D.E. Discher, Matrix Elasticity Directs Stem Cell Lineage Specification, Cell. 126 (2006) 677–689. doi:10.1016/j.cell.2006.06.044.
[3] J. Solon, I. Levental, K. Sengupta, P.C. Georges, P.A. Janmey, Fibroblast Adaptation and Stiffness Matching to Soft Elastic Substrates, Biophys J. 93 (2007) 4453–4461. doi:10.1529/biophysj.106.101386.
[4] O. Chaudhuri, L. Gu, D. Klumpers, M. Darnell, S.A. Bencherif, J.C. Weaver, N. Huebsch, H. Lee, E. Lippens, G.N. Duda, D.J. Mooney, Hydrogels with tunable stress relaxation regulate stem cell fate and activity, Nat Mater. 15 (2016) 326–334. doi:10.1038/nmat4489.
[5] O. Chaudhuri, Viscoelastic hydrogels for 3D cell culture, Biomater. Sci. 5 (2017) 1480–1490. doi:10.1039/C7BM00261K.
[6] A.R. Cameron, J.E. Frith, G.A. Gomez, A.S. Yap, J.J. Cooper-White, The effect of time-dependent deformation of viscoelastic hydrogels on myogenic induction and Rac1 activity in mesenchymal stem cells, Biomaterials. 35 (2014) 1857–1868. doi:10.1016/j.biomaterials.2013.11.023.
[7] A.R. Cameron, J.E. Frith, J.J. Cooper-White, The influence of substrate creep on mesenchymal stem cell behaviour and phenotype, Biomaterials. 32 (2011) 5979–5993. doi:10.1016/j.biomaterials.2011.04.003.
[8] A. Bauer, L. Gu, B. Kwee, W.A. Li, M. Dellacherie, A.D. Celiz, D.J. Mooney, Hydrogel substrate stress-relaxation regulates the spreading and proliferation of mouse myoblasts, Acta Biomater. 62 (2017) 82–90. doi:10.1016/j.actbio.2017.08.041.
[9] H. Lee, L. Gu, D.J. Mooney, M.E. Levenston, O. Chaudhuri, Mechanical confinement regulates cartilage matrix formation by chondrocytes, Nature Materials. (2017) nmat4993. doi:10.1038/nmat4993.
[10] M.-S. Hosseini, A.A. Katbab, Effects of surface viscoelasticity on cellular responses of endothelial cells, Rep Biochem Mol Biol. 3 (2014) 20–28.
[11] M. Murrell, R. Kamm, P. Matsudaira, Substrate viscosity enhances correlation in epithelial sheet movement, Biophys. J. 101 (2011) 297–306. doi:10.1016/j.bpj.2011.05.048.
[12] S.R. Peyton, P.D. Kim, C.M. Ghajar, D. Seliktar, A.J. Putnam, The effects of matrix stiffness and RhoA on the phenotypic plasticity of smooth muscle cells in a 3-D biosynthetic hydrogel system, Biomaterials. 29 (2008) 2597–2607. doi:10.1016/j.biomaterials.2008.02.005.
[13] T.A. Ulrich, E.M. de J. Pardo, S. Kumar, The Mechanical Rigidity of the Extracellular Matrix Regulates the Structure, Motility, and Proliferation of Glioma Cells, Cancer Res. 69 (2009) 4167–4174. doi:10.1158/0008-5472.CAN-08-4859.
[14] A. Valenzuela-Fernández, J.R. Cabrero, J.M. Serrador, F. Sánchez-Madrid, HDAC6: a key regulator of cytoskeleton, cell migration and cell–cell interactions, Trends in Cell Biology. 18 (2008) 291–297. doi:10.1016/j.tcb.2008.04.003.

[15] A.C. Brown, V.F. Fiore, T.A. Sulchek, T.H. Barker, Physical and chemical microenvironmental cues orthogonally control the degree and duration of fibrosis-associated epithelial-to-mesenchymal transitions, J. Pathol. 229 (2013) 25–35. doi:10.1002/path.4114.
[16] A.J. Booth, R. Hadley, A.M. Cornett, A.A. Dreffs, S.A. Matthes, J.L. Tsui, K. Weiss, J.C. Horowitz, V.F. Fiore, T.H. Barker, B.B. Moore, F.J. Martinez, L.E. Niklason, E.S. White, Acellular Normal and Fibrotic Human Lung Matrices as a Culture System for In Vitro Investigation, Am J Respir Crit Care Med. 186 (2012) 866–876. doi:10.1164/rccm.201204-0754OC.
[17] P.-J. Wipff, D.B. Rifkin, J.-J. Meister, B. Hinz, Myofibroblast contraction activates latent TGF-β1 from the extracellular matrix, The Journal of Cell Biology. 179 (2007) 1311–1323.
[18] A. Leask, A. Holmes, D.J. Abraham, Connective tissue growth factor: A new and important player in the pathogenesis of fibrosis, Curr Rheumatol Rep. 4 (2002) 136–142. doi:10.1007/s11926-002-0009-x.
[19] A.B. South, L.A. Lyon, Autonomic self-healing of hydrogel thin films, Angew. Chem. Int. Ed. Engl. 49 (2010) 767–771. doi:10.1002/anie.200906040.
[20] S. Saxena, C.E. Hansen, L.A. Lyon, Microgel Mechanics in Biomaterial Design, Accounts of Chemical Research. 47 (2014) 2426–2434.
[21] S. Saxena, M.W.S. Jr, H. Yoshida, J.C. Gaulding, A.J. García, L.A. Lyon, Microgel film dynamics modulate cell adhesion behavior, Soft Matter. 10 (2014) 1356–1364. doi:10.1039/C3SM52518J.
[22] C.M. Nolan, C.D. Reyes, J.D. Debord, A.J. García, L.A. Lyon, Phase Transition Behavior, Protein Adsorption, and Cell Adhesion Resistance of Poly(ethylene glycol) Cross-Linked Microgel Particles, Biomacromolecules. 6 (2005) 2032–2039. doi:10.1021/bm0500087.
[23] M.W. Spears, E.S. Herman, J.C. Gaulding, L.A. Lyon, Dynamic Materials from Microgel Multilayers, Langmuir. 30 (2014) 6314–6323. doi:10.1021/la403058t.
[24] H. Bachman, A.C. Brown, K.C. Clarke, K.S. Dhada, A. Douglas, C.E. Hansen, E. Herman, J.S. Hyatt, P. Kodlekere, Z. Meng, S. Saxena, M.W. Spears, N. Welsch, L.A. Lyon, Ultrasoft, highly deformable microgels, Soft Matter. 11 (2015) 2018–2028. doi:10.1039/c5sm00047e.
[25] A. Joshi, S. Nandi, D. Chester, A.C. Brown, M. Muller, Study of poly (N-isopropylacrilamide-co-acrylic acid) (pNIPAM) microgel particle induced deformations of tissue mimicking phantom by ultrasound stimulation, Langmuir. (2017). doi:10.1021/acs.langmuir.7b02801.
[26] E.P. Sproul, S. Nandi, C. Roosa, L. Schreck, A.C. Brown, Biomimetic Microgels with Controllable Deformability Improve Healing Outcomes, Advanced Biosystems. 0 (2018) 1800042. doi:10.1002/adbi.201800042.
[27] ASCB EMBO 2017 Poster: Efficient microscopy image visualization and cell tracking analysis of multi-gigabyte datasets| Microscopy image analysis software, DRVISION | Microscopy Image Analysis Software. (n.d.). https://www.drvtechnologies.com/single-post/2017/12/06/ASCB-EMBO-2017-Poster-Efficient-microscopy-image-visualization-and-cell-tracking-analysis-of-multi-gigabyte-datasets (accessed January 4, 2018).
[28] D. Chester, A.C. Brown, The role of biophysical properties of provisional matrix proteins in wound repair, Matrix Biology. 60 (2017) 124–140. doi:10.1016/j.matbio.2016.08.004.
[29] B. Hinz, Matrix mechanics and regulation of the fibroblast phenotype, Periodontol 2000. 63 (2013) 14–28. doi:10.1111/prd.12030.
[30] J.J. Tomasek, G. Gabbiani, B. Hinz, C. Chaponnier, R.A. Brown, Myofibroblasts and mechano-regulation of connective tissue remodelling, Nature Reviews Molecular Cell Biology. 3 (2002) 349. doi:10.1038/nrm809.
[31] R. Akhtar, H.K. Graham, B. Derby, M.J. Sherratt, A.W. Trafford, R.S. Chadwick, N. Gavara, Frequency-modulated atomic force microscopy localises viscoelastic remodelling in the ageing sheep aorta, Journal of the Mechanical Behavior of Biomedical Materials. 64 (2016) 10–17. doi:10.1016/j.jmbbm.2016.07.018.

[32] J. Rother, H. Nöding, I. Mey, A. Janshoff, Atomic force microscopy-based microrheology reveals significant differences in the viscoelastic response between malign and benign cell lines, Open Biol. 4 (2014). doi:10.1098/rsob.140046.
[33] J. Alcaraz, L. Buscemi, M. Grabulosa, X. Trepat, B. Fabry, R. Farré, D. Navajas, Microrheology of human lung epithelial cells measured by atomic force microscopy, Biophys. J. 84 (2003) 2071–2079. doi:10.1016/S0006-3495(03)75014-0.
[34] D.G. Yablon, J. Grabowski, I. Chakraborty, Measuring the loss tangent of polymer materials with atomic force microscopy based methods, Meas. Sci. Technol. 25 (2014) 055402. doi:10.1088/0957-0233/25/5/055402.
[35] M. Yin, K.J. Glaser, A. Manduca, T. Mounajjed, H. Malhi, D.A. Simonetto, R. Wang, L. Yang, S.A. Mao, J.M. Glorioso, F.M. Elgilani, C.J. Ward, P.C. Harris, S.L. Nyberg, V. Shah, R.L. Ehman, Distinguishing between Hepatic Inflammation and Fibrosis with Magnetic Resonance Elastography, Radiology. 284 (2017) 694–705. doi:10.1148/radiol.2017160622.
[36] T. Lämmermann, M. Sixt, Mechanical modes of "amoeboid" cell migration, Curr. Opin. Cell Biol. 21 (2009) 636–644. doi:10.1016/j.ceb.2009.05.003.
[37] P. Friedl, S. Borgmann, E.-B. Bröcker, Amoeboid leukocyte crawling through extracellular matrix: lessons from the Dictyostelium paradigm of cell movement, Journal of Leukocyte Biology. 70 (2001) 491–509. doi:10.1189/jlb.70.4.491.
[38] G. Charras, E. Paluch, Blebs lead the way: how to migrate without lamellipodia, Nature Reviews Molecular Cell Biology. 9 (2008) 730–736. doi:10.1038/nrm2453.
[39] P. Friedl, Prespecification and plasticity: shifting mechanisms of cell migration, Current Opinion in Cell Biology. 16 (2004) 14–23. doi:10.1016/j.ceb.2003.11.001.
[40] P. Friedl, K. Wolf, Plasticity of cell migration: a multiscale tuning model, The Journal of Cell Biology. (2009) jcb.200909003. doi:10.1083/jcb.200909003.
[41] X. Trepat, Z. Chen, K. Jacobson, Cell Migration, Compr Physiol. 2 (2012) 2369–2392. doi:10.1002/cphy.c110012.
[42] N.V. Krakhmal, M.V. Zavyalova, E.V. Denisov, S.V. Vtorushin, V.M. Perelmuter, Cancer Invasion: Patterns and Mechanisms, Acta Naturae. 7 (2015) 17–28.
[43] K. Wolf, I. Mazo, H. Leung, K. Engelke, U.H. von Andrian, E.I. Deryugina, A.Y. Strongin, E.-B. Bröcker, P. Friedl, Compensation mechanism in tumor cell migration: mesenchymal–amoeboid transition after blocking of pericellular proteolysis, The Journal of Cell Biology. 160 (2003) 267–277. doi:10.1083/jcb.200209006.
[44] V. Sanz-Moreno, G. Gadea, J. Ahn, H. Paterson, P. Marra, S. Pinner, E. Sahai, C.J. Marshall, Rac activation and inactivation control plasticity of tumor cell movement, Cell. 135 (2008) 510–523. doi:10.1016/j.cell.2008.09.043.
[45] E. Sahai, C.J. Marshall, Differing modes of tumour cell invasion have distinct requirements for Rho/ROCK signalling and extracellular proteolysis, Nat. Cell Biol. 5 (2003) 711–719. doi:10.1038/ncb1019.
[46] C.D. Nobes, A. Hall, Rho GTPases Control Polarity, Protrusion, and Adhesion during Cell Movement, The Journal of Cell Biology. 144 (1999) 1235–1244. doi:10.1083/jcb.144.6.1235.
[47] G. Totsukawa, Y. Wu, Y. Sasaki, D.J. Hartshorne, Y. Yamakita, S. Yamashiro, F. Matsumura, Distinct roles of MLCK and ROCK in the regulation of membrane protrusions and focal adhesion dynamics during cell migration of fibroblasts, The Journal of Cell Biology. 164 (2004) 427–439. doi:10.1083/jcb.200306172.
[48] V. Sanz-Moreno, C.J. Marshall, The plasticity of cytoskeletal dynamics underlying neoplastic cell migration, Current Opinion in Cell Biology. 22 (2010) 690–696. doi:10.1016/j.ceb.2010.08.020.
[49] D. Duscher, Z.N. Maan, V.W. Wong, R.C. Rennert, M. Januszyk, M. Rodrigues, M. Hu, A.J. Whitmore, A.J. Whittam, M.T. Longaker, G.C. Gurtner, Mechanotransduction and fibrosis, J Biomech. 47 (2014) 1997–2005. doi:10.1016/j.jbiomech.2014.03.031.

[50] W. Carver, E.C. Goldsmith, W. Carver, E.C. Goldsmith, Regulation of Tissue Fibrosis by the Biomechanical Environment, BioMed Research International, BioMed Research International. 2013, 2013 (2013) e101979. doi:10.1155/2013/101979, 10.1155/2013/101979.
[51] J.J. Tomasek, M.B. Vaughan, B.P. Kropp, G. Gabbiani, M.D. Martin, C.J. Haaksma, B. Hinz, Contraction of myofibroblasts in granulation tissue is dependent on Rho/Rho kinase/myosin light chain phosphatase activity, Wound Repair and Regeneration. 14 (2006) 313–320. doi:10.1111/j.1743-6109.2006.00126.x.
[52] A.B. South, R.E. Whitmire, A.J. García, L.A. Lyon, Centrifugal deposition of microgels for the rapid assembly of nonfouling thin films, ACS Appl Mater Interfaces. 1 (2009) 2747–2754. doi:10.1021/am9005435.
[53] X. Hu, L.A. Lyon, Thin Films Constructed by Centrifugal Deposition of Highly Deformable, Charged Microgels, ACS Macro Lett. 4 (2015) 302–307. doi:10.1021/acsmacrolett.5b00016.
[54] J.C. Gaulding, M.W. Spears, L.A. Lyon, Plastic deformation, wrinkling, and recovery in microgel multilayers, Polym Chem. 4 (2013) 4890–4896. doi:10.1039/C3PY00173C.
[55] L. Zhang, M.W. Spears, L.A. Lyon, Tunable Swelling and Rolling of Microgel Membranes, Langmuir. 30 (2014) 7628–7634. doi:10.1021/la500860t.
[56] K. Gauthaman, C.-Y. Fong, A. Bongso, Effect of ROCK Inhibitor Y-27632 on Normal and Variant Human Embryonic Stem Cells (hESCs) In Vitro: Its Benefits in hESC Expansion, Stem Cell Rev and Rep. 6 (2010) 86–95. doi:10.1007/s12015-009-9107-8.
[57] Y. Gao, J.B. Dickerson, F. Guo, J. Zheng, Y. Zheng, Rational design and characterization of a Rac GTPase-specific small molecule inhibitor, PNAS. 101 (2004) 7618–7623. doi:10.1073/pnas.0307512101.
[58] Z. Surviladze, A. Waller, J.J. Strouse, C. Bologa, O. Ursu, V. Salas, J.F. Parkinson, G.K. Phillips, E. Romero, A. Wandinger-Ness, L.A. Sklar, C. Schroeder, D. Simpson, J. Nöth, J. Wang, J. Golden, J. Aubé, A Potent and Selective Inhibitor of Cdc42 GTPase, in: Probe Reports from the NIH Molecular Libraries Program, National Center for Biotechnology Information (US), Bethesda (MD), 2010. http://www.ncbi.nlm.nih.gov/books/NBK51965/.
[59] R.A. McCloy, S. Rogers, C.E. Caldon, T. Lorca, A. Castro, A. Burgess, Partial inhibition of Cdk1 in G2 phase overrides the SAC and decouples mitotic events, Cell Cycle. 13 (2014) 1400–1412. doi:10.4161/cc.28401.
[60] J.R. Tse, A.J. Engler, Preparation of hydrogel substrates with tunable mechanical properties, Curr Protoc Cell Biol. Chapter 10 (2010) Unit 10.16. doi:10.1002/0471143030.cb1016s47.
[61] I. Muhamed, J. Wu, P. Sehgal, X. Kong, A. Tajik, N. Wang, D.E. Leckband, E-cadherin-mediated force transduction signals regulate global cell mechanics, J Cell Sci. 129 (2016) 1843–1854. doi:10.1242/jcs.185447.
[62] M. Takeichi, S. Nakagawa, Cadherin-dependent cell-cell adhesion, Curr Protoc Cell Biol. Chapter 9 (2001) Unit 9.3. doi:10.1002/0471143030.cb0903s00.
[63] J.P. Butler, I.M. Tolić-Nørrelykke, B. Fabry, J.J. Fredberg, Traction fields, moments, and strain energy that cells exert on their surroundings, Am. J. Physiol., Cell Physiol. 282 (2002) C595-605. doi:10.1152/ajpcell.00270.2001.
[64] J.H.-C. Wang, J.-S. Lin, Cell traction force and measurement methods, Biomech Model Mechanobiol. 6 (2007) 361. doi:10.1007/s10237-006-0068-4.

Figures

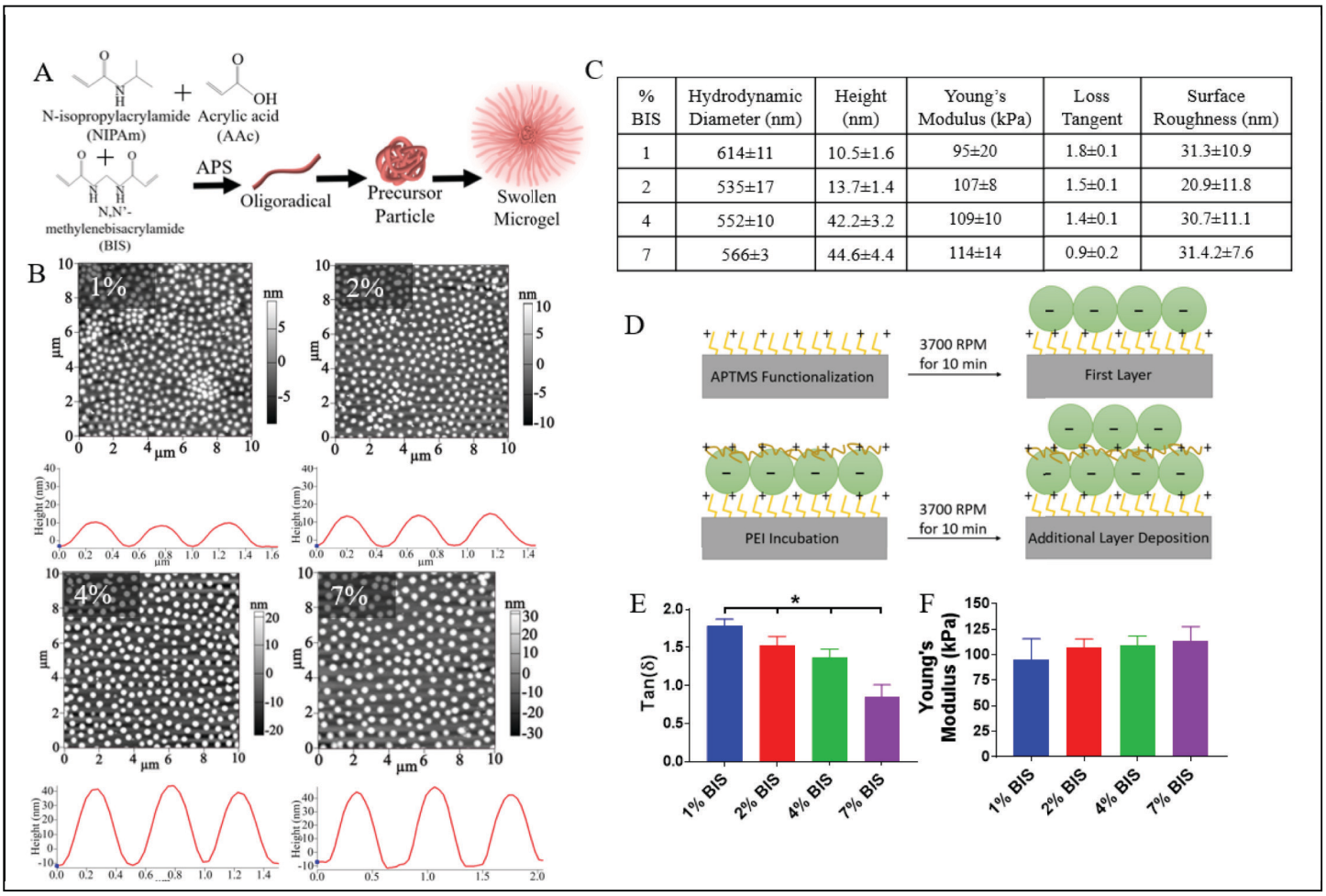

% BIS	Hydrodynamic Diameter (nm)	Height (nm)	Young's Modulus (kPa)	Loss Tangent	Surface Roughness (nm)
1	614±11	10.5±1.6	95±20	1.8±0.1	31.3±10.9
2	535±17	13.7±1.4	107±8	1.5±0.1	20.9±11.8
4	552±10	42.2±3.2	109±10	1.4±0.1	30.7±11.1
7	566±3	44.6±4.4	114±14	0.9±0.2	31.4.2±7.6

Figure 1. Characterization of microgel thin film properties: A) Microgel particles are created in a precipitation-polymerization reaction with the constituents p-NIPam, AAc, and BIS and initiated with APS at 70°C. Microgel particles were created by keeping the AAc concentration at 5% and by varying the amount of BIS to be either 1, 2, 4, or 7%. B) Dry microgel particle diameters and heights were measured with AFM. C) Summary of microgel particle and film characterization. D) Microgel thin films were created in a LBL process through centrifugation where layers of negatively charged microgel particles were alternated with layers of positively charged PEI. E) Film loss tangent was measure through AFM. F) The Young's Modulus of each film was measured with AFM and data was fit with the Hertz model; * $p<0.05$

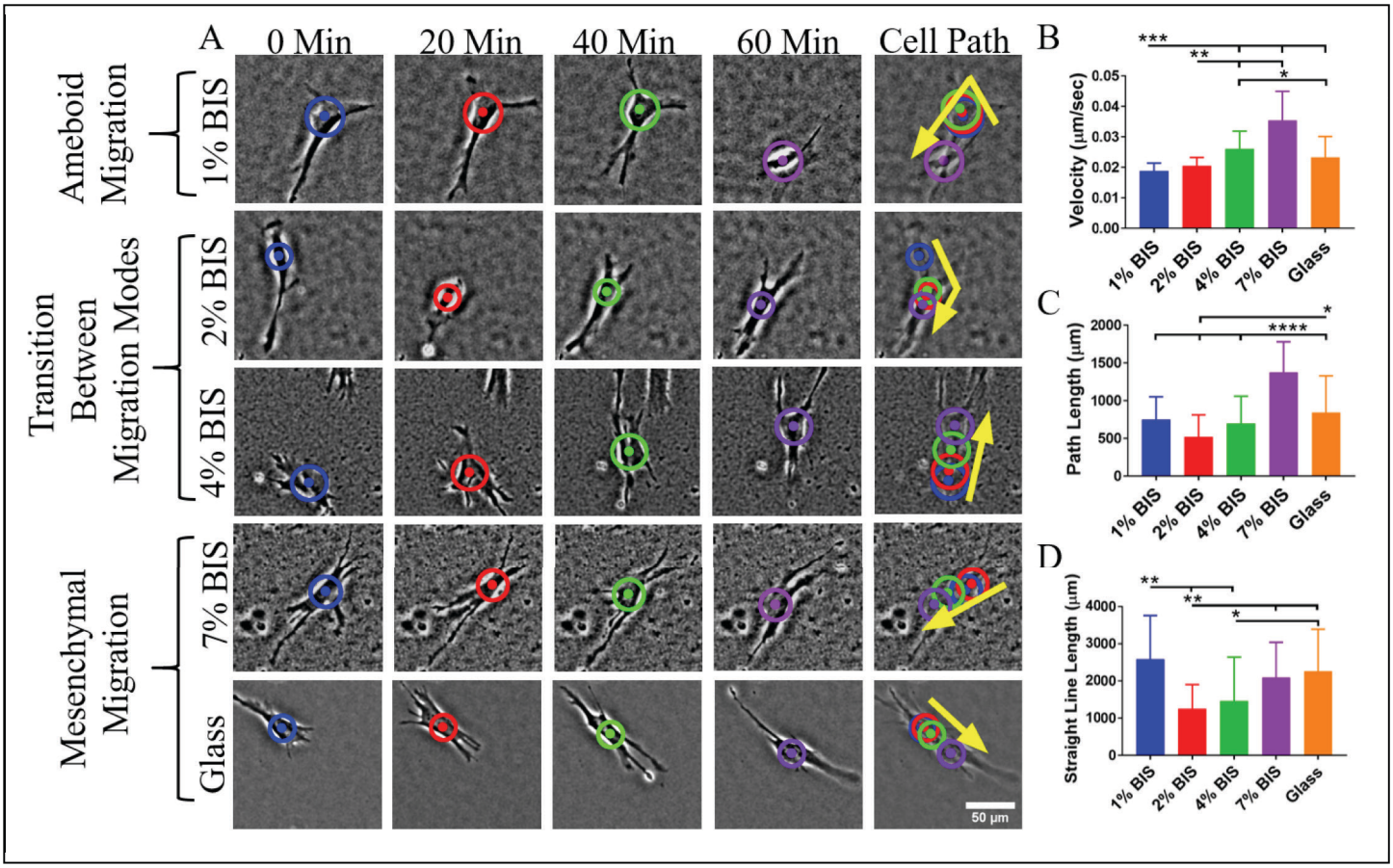

Figure 2. Analysis of fibroblast migration responses on microgel thin films: HDFns were seeded on collagen coated microgel thin films for 2 hrs and imaged over 24 hrs. A) Representative images of single cells migrating using either ameboid or mesenchymal cell migration over 60 mins are shown. Circles represent the cell body, while the dots represent the centroid of the cell body. Yellow arrows represent direction and relative path of migration. The time-lapse videos were then analyzed in the commercially available software Aivia to quantify cellular migration responses including velocity (B), path length (C), and straight-line length (D). * $p<0.05$; ** $p<0.01$; *** $p<0.001$; **** $p<0.0001$.

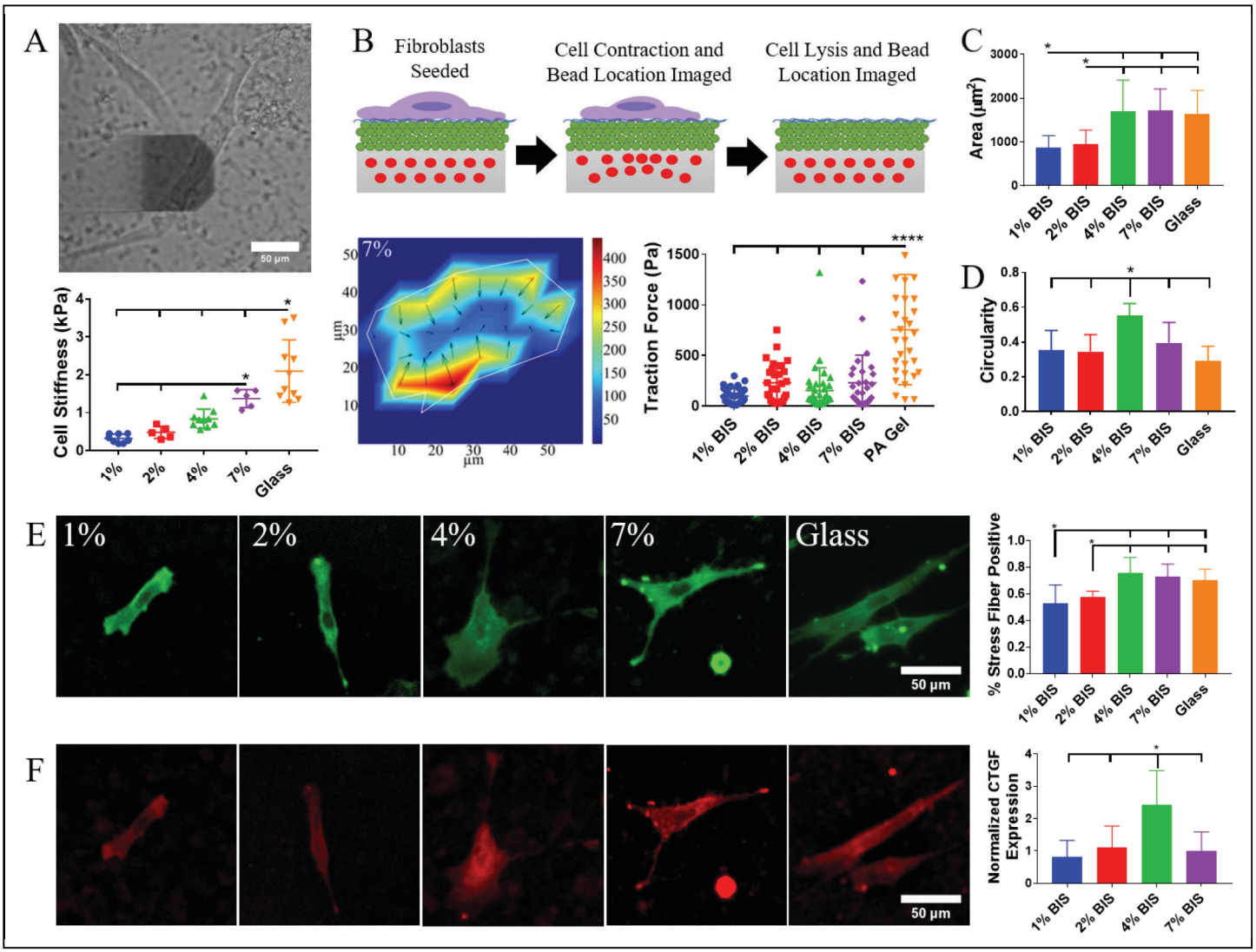

Figure 3. Loss tangent of microgel films modulates cell contractility, morphology, stress fiber formation, and CTGF Expression: A) HDFns were seeded on collagen coated microgel films and single cell stiffness was measured 12 hrs after seeding via AFM. B) TFM was performed on a cell-by-cell basis with cells seeded on collagen coated films built on PA gels containing fluorescent beads. 12 hrs after seeding images were taken of individual cells before and after lysis. Traction forces were calculated using a MatLab algorithm. HDFns were seeded on collagen coated films for 24 hrs and then stained for α-SMA (E) and CTGF (F). Cell area (C), circularity (D), the percent of stress fiber positive cells (E) and CTGF expression (F) were quantified in ImageJ. * $p<0.05$

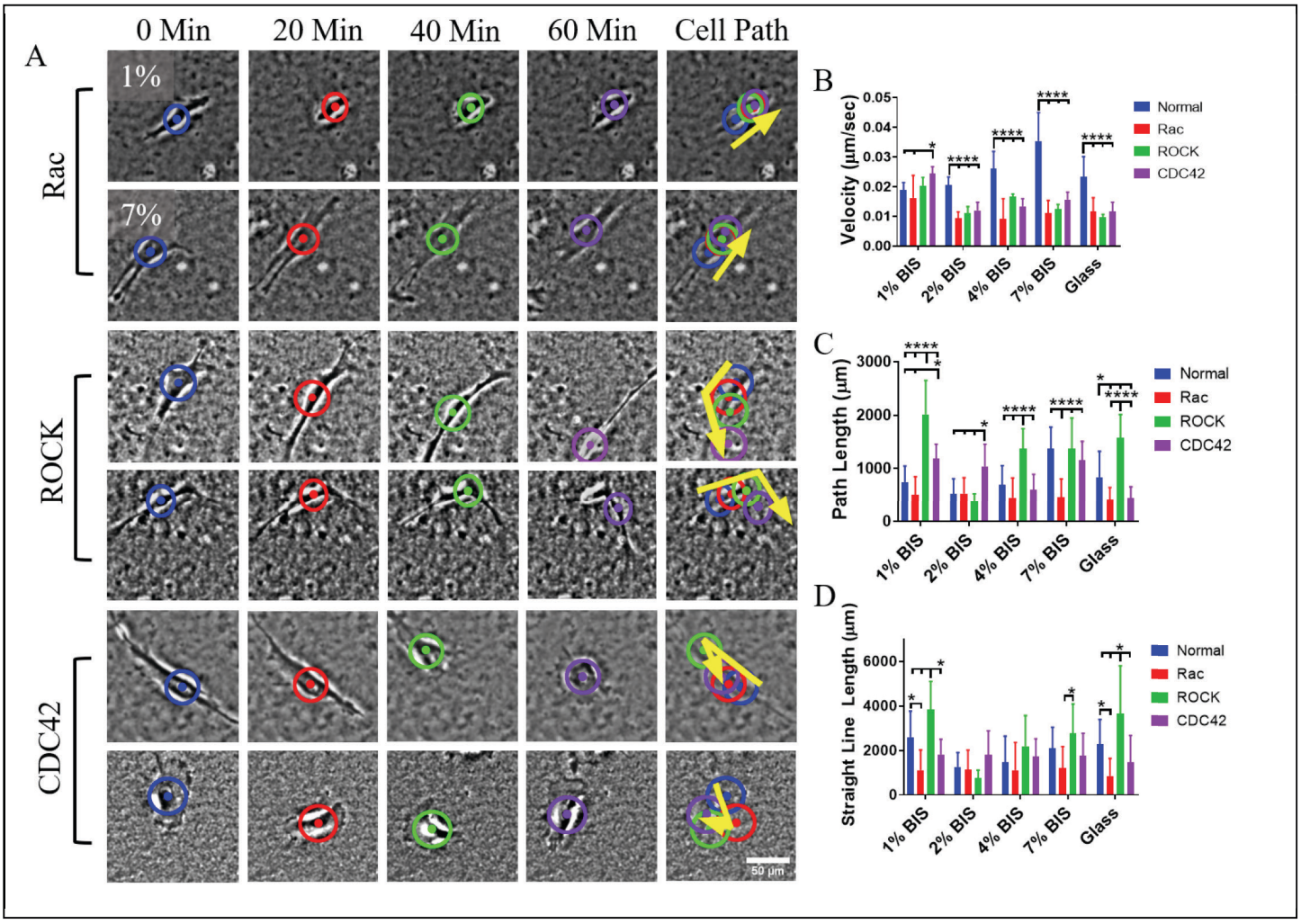

Figure 4. Analysis of the contribution of RAC, ROCK, and CDC42 pathways on fibroblast migration responses on microgel thin films: HDFns were seeded on collagen coated microgel films and allowed to attach for 2 hrs before the addition of either a CDC42, Rac1, or ROCK contractility inhibitor. Cells were imaged over 24 hrs. A) Representative images of single cells migrating using either ameboid or mesenchymal cell migration over 60 min on each film are shown. Circles represent the cell body, while the dots represent the centroid of the cell body. Yellow arrows represent direction and relative path of migration. Time-lapse videos were analyzed in the commercially available software Aivia to quantify cellular migration responses including velocity (B), path length (C), and straight line length (D). * $p<0.05$; **** $p<0.0001$

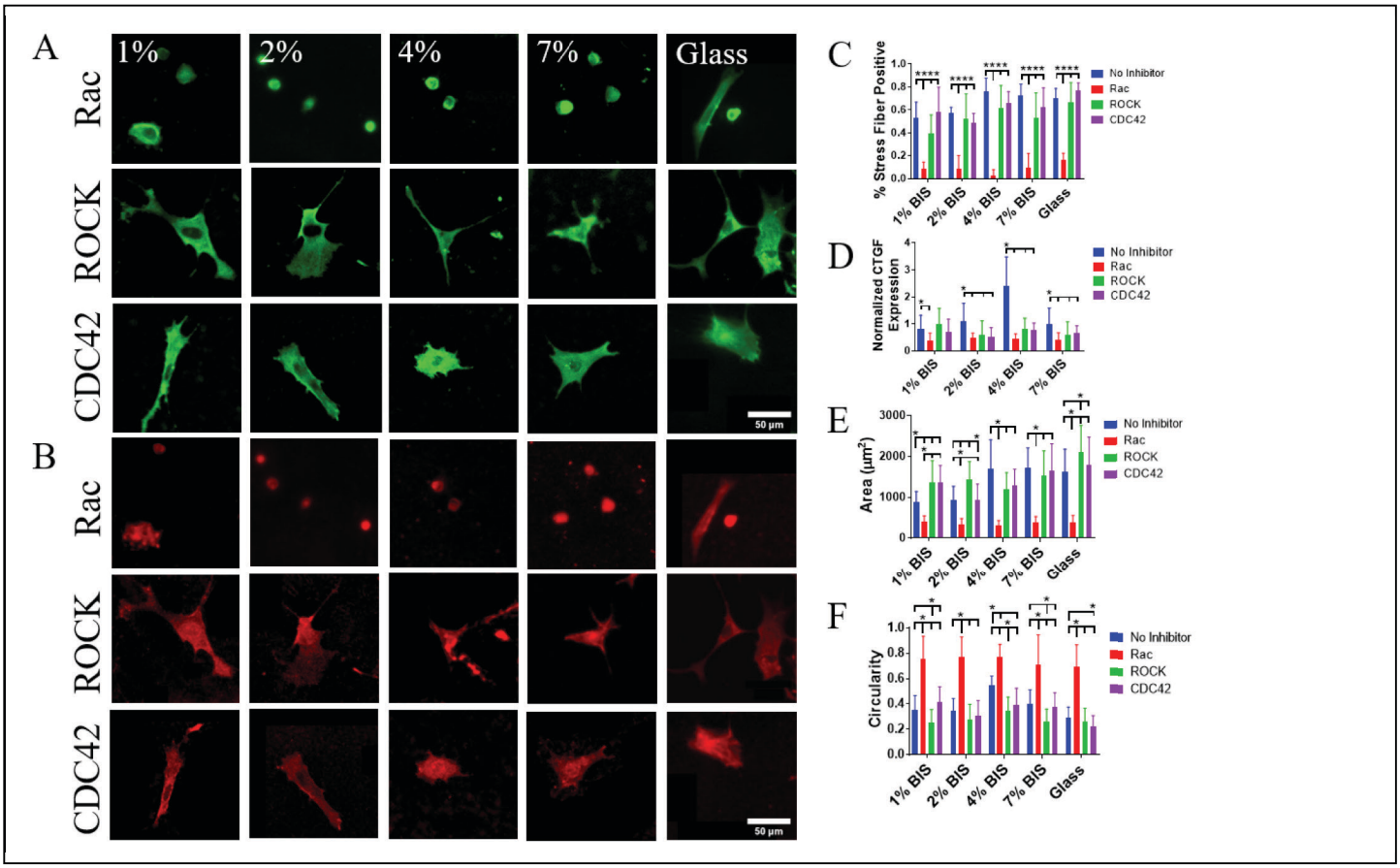

Figure 5. Contractility inhibitors normalize cell morphology and CTGF expression: HDFns were seeded on collagen coated microgel films and allowed to attach for 2 hrs before the addition of a CDC42, Rac1, or ROCK contractility inhibitor and then incubated for 24 hrs. Cells were stained for α-SMA (A) and CTGF (B) and imaged. The percent of stress fiber positive cells (C), CTGF expression (D), cell area (E), and circularity (F) were measured using ImageJ. * $p<0.05$; **** $p<0.0001$

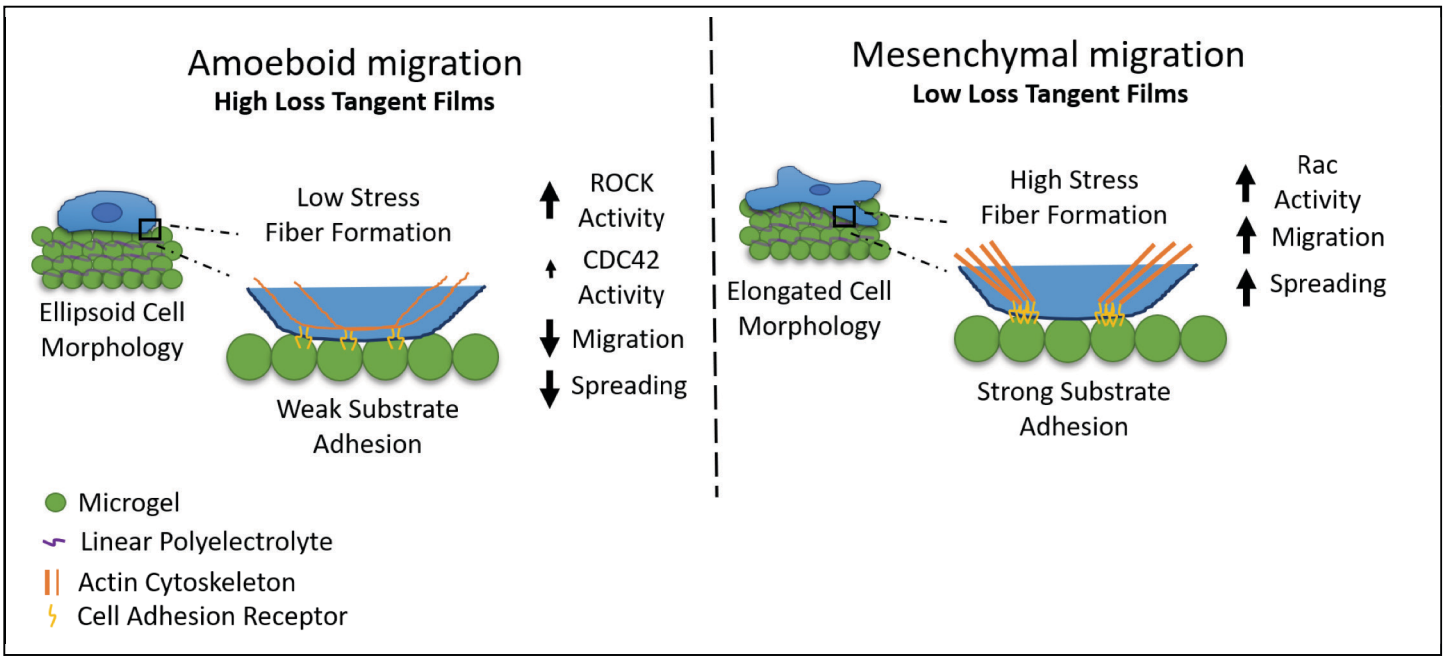

Figure 6. Overview of the effect of film loss tangent on cell migration: Film loss tangent influences the fibroblast mode of migration. As film loss tangent increased, amoeboid migration was seen to be the dominate mode of cell migration. Amoeboid migration is characterized by round or ellipsoid cells that have poor stress fiber formation and are loosely attached to the surface. On low loss tangent films, mesenchymal cell migration was the dominate mode of cell migration. Mesenchymal migration is characterized by highly spread and elongated cells that have high degrees of stress fiber formation and strong adhesions to the surface. Upon adding the cell contractility inhibitors for Rac, ROCK, and CDC42, it was observed that both ROCK and CDC42 signaling plays an important role in amoeboid migration, while Rac signaling is important for mesenchymal migration.